Surf Zone Longshore Currents and Random Waves: Field Data and Models

EDWARD B. THORNTON

Oceanography Department, Naval Postgraduate School, Monterey, CA 93944

R. T. GUZA

Center for Coastal Studies, Scripps Institution of Oceanography, University of California, La Jolla, CA 92037

(Manuscript received 25 February 1985, in final form 18 December 1985)

ABSTRACT

Analytic and numerical models for longshore currents generated by obliquely incident random waves are compared with field observations. Five days of observations were selected during which the waves were narrow banded in both frequency and direction, in keeping with model assumptions. The extensive measurements included radiation stress and wave directional spectra in 9 m depth, and a closely spaced array of current and pressure sensors on a line perpendicular to shore. The longshore current models are based on balancing the gradient of the radiation stress with the alongshore bed shear and Reynold's stresses, assuming stationary wave conditions and straight and parallel bottom contours. The spatial variation of wave height, required to determine the gradient of the radiation stress, is modeled using linear random wave theory. Given H_{rms} in 9 m depth, the model predicts H_{rms} at shoreward locations with an average error of less than 9%. Using a nonlinear bottom shear stress formulation and the measured topography, a bed shear stress coefficient of $c_f = 0.006$ gives optimal agreement between observed and predicted longshore currents. Eddy viscosity was found not to be important, at least for the nearly planar topography present during the observations.

1. Introduction

The modern theories for mean longshore currents due to oblique wave approach are based on a longshore momentum flux balance (Bowen, 1969; Thornton, 1970; Longuet-Higgins, 1970a,b). Although a number of refinements have evolved since these earlier models, most models still describe the waves as monochromatic. In addition, there are only a limited number of high quality laboratory and field experiments with which to test the various models.

In the simplest models (and in selected field data at Leadbetter Beach, California) the waves are stationary and the bottom contours straight and parallel. The time averaged equation for longshore momentum simplifies to a local balance between the on–offshore gradient of the longshore momentum flux due to unsteady motion and the longshore bottom stress, $\tau_y{}^b$,

$$\frac{\partial S_{yx}}{\partial x} = -\tau_y{}^b; \tag{1}$$

S_{yx} is the time and depth averaged covariance between the unsteady velocity components

$$S_{yx} = \tilde{S}_{yx} + S'_{yx} = \overline{\int_{-h}^{\eta} \rho \tilde{u}\tilde{v} dz} + \overline{\int_{-h}^{\eta} \rho u'v' dz} \tag{2}$$

where ($\tilde{}$) and prime refer to wave and turbulent components. It has been assumed in (2) that the wave-induced and turbulent velocity components are statistically independent, which appears to be a reasonable assumption within the surf zone (Thornton, 1979). The first term on the rhs of (2) is the wave induced momentum flux (commonly referred to as the radiation stress) and the second term represents the depth integrated turbulent Reynold's stress.

In monochromatic models, the waves outside the surf zone do not break. All waves initially break at the same location; shoreward of this break point the wave energy decreases as $H = \gamma h$. Outside the surf zone $\tilde{S}_{yx}$ is conserved and the driving force for longshore currents is zero. At the break point, the waves suddenly begin to lose energy and there is an abrupt change in the gradient of $\tilde{S}_{yx}$. The resulting longshore current distribution is no current outside the surf zone, a maximum current at the break point and then a gradual decrease to zero current at the beach. To smooth the physically unrealistic current shear at the breakerline, it is necessary to introduce an eddy viscosity term parameterizing the lateral turbulent momentum exchange, S'_{yx}.

An alternative formulation appropriate for random waves (i.e., field situations) is to describe the wave heights in terms of a probability distribution (Collins, 1970; Battjes, 1972). At each cross-shore location in a transect there is a distribution of wave heights, and also a distribution of breaking wave heights. Only a few waves break offshore. Closer to the beach, more

© 1986 American Meteorological Society

and more waves of the distribution are breaking, until in the inner surf zone almost all the waves are breaking ("saturation"). Hence, there is not a single sharp breakerline. The waves break over a large region with increasing intensity towards the beach. The spreading out of the breakerline results in smooth changes in the rate of energy dissipation and $\tilde{S}_{yx}$. The resulting longshore currents also have a smooth profile. The need to include an eddy viscosity to smooth out the velocity profile is reduced, or eliminated (Collins, 1970; Battjes, 1972).

In this paper, a narrow-band, random wave transformation model (Thornton and Guza, 1983) is used to describe the wave spatial transformation required in the longshore current formulation. An analytical model describing the cross-shore distribution of longshore currents for plane sloping beaches, as well as numerical models for general bottom profiles are developed. The waves and currents measured at Leadbetter Beach, California are described in detail and are used to test the wave transformation and longshore current models. This dataset affords the first reasonable test for random wave generated longshore current models.

Wu et al. (1985) compared a monochromatic, two-dimensional, finite-element model with the same data. This model included the nonlinear advective terms in the momentum equation and the effects of longshore topographic inhomogeneities. Nonlinear advective terms were shown to not be a dominant effect. The importance of longshore topographic inhomogeneities has been assessed by running the two-dimensional model for waves approaching normal to the shoreline; the resulting currents were small (<5 cm s^{-1}), indicating that longshore inhomogeneities in the nearshore current and wave fields induced by the bathymetry are weak (C. S. Wu, personal communication, 1984).

2. Models

a. *Wave height transformation*

The wave height transformation model of Thornton and Guza (1983), which is an extension of the earlier work by Battjes and Janssen (1978), is summarized here because it is an integral part of the longshore current model, and has not been previously applied to the present dataset. Assuming wave stationarity and straight and parallel contours, the energy flux balance equation is given by

$$\frac{dEC_g \cos\hat{\alpha}}{dx} = \langle \epsilon_b \rangle \tag{3}$$

where E is the energy density, $C_g \cos\hat{\alpha}$ is the shoreward component of group velocity, $\hat{\alpha}$ is a mean wave direction, and $\langle \epsilon_b \rangle$ is the ensemble averaged dissipation due to wave breaking. Dissipation due to bottom friction could also be included in the analysis, but was shown by Thornton and Guza (1983) to be negligible compared with dissipation due to wave-breaking approaching or within the surf zone.

The dissipation function $\langle \epsilon_b \rangle$ is only applied to the breaking waves, and it is therefore necessary to identify which waves are breaking. The observations of Thornton and Guza (1983) motivated their model in which Rayleigh distributed offshore wave heights were modified by shoaling and breaking into new distributions which were again nearly Rayleigh, but with some energy loss. The distribution of breaking waves describes which waves of the Rayleigh distribution are breaking, and is expressed as a weighting of the Rayleigh pdf $[p(H)]$

$$p_b(H) = W(H)p(H) \tag{4}$$

where the weighting function $W(H) \leq 1$. The weighting function should have the characteristics that no waves break in deep water, $W(H) \to 0$ as $h \to \infty$, and all waves break in the inner surf zone, $W(H) \to 1$ as $h \to 0$. An algebraically simple form for $W(h)$ which does a reasonable job of predicting the fraction of waves that break from offshore to saturation conditions is

$$W(H) = \left(\frac{H_{\text{rms}}}{\gamma h}\right)^4 \tag{5}$$

where h is the local water depth and γ is based on the field data in the saturated inner surf zone. More complicated forms for $W(H)$, which make the larger waves (at a given depth) more likely to break, lead to results similar to the simpler model discussed here.

The dissipation due to wave breaking $\langle \epsilon_b \rangle$ is modeled as a simple periodic linear bore (Hwang and Divoky, 1970). The average rate of energy dissipation is calculated by multiplying the dissipation for a single broken wave of height H by the probability of wave breaking at each height $[p_b(H)]$, and integrating for all H. The resulting average dissipation is (Thornton and Guza, 1983)

$$\langle \epsilon_b \rangle = \frac{3}{16}\sqrt{\pi}\,\rho g \frac{B^3}{\gamma^4 h^5} f_p H_{\text{rms}}^7 \tag{6}$$

where the frequency f_p corresponds to the peak of the narrowband energy spectrum. The coefficient B, determined from the wave height data, accounts for the differences in various breaker types, and would be expected to be less than one for spilling breakers and near unity for full plunging breakers.

The energy flux, EC_g, in (3) is approximated using linear theory for C_g at frequency f_p and

$$E = \frac{1}{8}\rho g \int_0^\infty H^2 p(H) dH = \frac{1}{8}\rho g H_{\text{rms}}^2. \tag{7}$$

Substitution of (6) and (7) in the energy balance (3) yields a first-order differential equation for the linear transformation model

$$\frac{d}{dx}\frac{1}{8}\rho g H_{\text{rms}}^2 C_g \cos\hat{\alpha} = \frac{3}{16}\sqrt{\pi}\,\rho g \frac{B^3}{\gamma^4 h^5} f_p H_{\text{rms}}^7. \tag{8}$$

For an arbitrary bottom profile, H_{rms} is determined by numerically integrating (8).

By assuming small incident wave angles ($\hat{\alpha} < 9°$, such that $\cos\hat{\alpha} \approx 1$), shallow water, and a plane beach with slope $\tan\beta$, Thornton and Guza (1983) obtained an analytical solution

$$H_{rms} = a^{1/5}h^{9/10}\left[1 - h^{23/4}\left(\frac{1}{h_0^{23/4}} - \frac{a}{r_0^{5/2}}\right)\right]^{-1/5}, \qquad 0 \leq h \leq h_0 \quad (9)$$

where

$$r_0 = H_0^2 h_0^{1/2}$$

$$a = \frac{23}{15}\left(\frac{g}{\pi}\right)^{1/2}\frac{\gamma^4 \tan\beta}{B^3 f_p}$$

and the subscript zero refers to the input conditions at the most offshore (but still shallow water) location.

b. Longshore currents

The time-averaged longshore current distribution across the surf zone is derived from (1). The radiation stress, to second order in wave slope, is described by (Longuet-Higgins and Stewart, 1964)

$$\tilde{S}_{yx} = EC_g \cos\hat{\alpha}\frac{\sin\hat{\alpha}}{C} \quad (10)$$

where $\hat{\alpha}$ is the mean angle of wave approach for the assumed very narrow band waves described by a peak frequency, f_p and random wave heights. The term

$$\frac{\sin\hat{\alpha}}{C} = \text{const} = \frac{\sin\hat{\alpha}_0}{C_0} \quad (11)$$

by Snell's law of linear wave refraction, so

$$\frac{d}{dx}\tilde{S}_{yx} = \frac{\sin\hat{\alpha}_0}{C_0}\frac{d}{dx}(EC_g\cos\hat{\alpha}) = \frac{\sin\hat{\alpha}_0}{C_0}\langle\epsilon_b\rangle \quad (12)$$

with the change in energy flux equal to the breaking wave dissipation $\langle\epsilon_b\rangle$ for straight and parallel contours (Eq. 3). The alongshore momentum equation (1) can now be written

$$\frac{\sin\hat{\alpha}_0}{C_0}\langle\epsilon_b\rangle = \frac{-d}{dx}S'_{yx} - \tau_y{}^b. \quad (13)$$

A hierarcy of solutions is considered to determine the relative importance of the terms on the rhs of (13). Solutions are derived for linearized and general formulations for the bottom shear stress, and with and without turbulent momentum exchange.

The simplest formulation neglects turbulent momentum exchange and incorporates a linearized bottom stress, and is derived first. The longshore component of the bed shear stress in (1) is modeled with a quadratic bottom shear stress law

$$\tau_y{}^b = \rho c_f\overline{|\vec{u}|}v \quad (14)$$

where $\vec{u}$ is the total instantaneous velocity, v is the total alongshore velocity and c_f is the bed shear stress coefficient. For the case of small angle of wave incidence and weak mean longshore current, i.e., $V/\overline{|\tilde{u}|} \ll 1$, the bottom shear stress simplifies to (Longuet-Higgins, 1970a; Thornton, 1970)

$$\tau_y{}^b = \rho c_f\overline{|\tilde{u}|}V \quad (15)$$

which linearizes the momentum equation (1) in terms of the mean longshore current, V, and allows an analytical solution. The wave velocity $\tilde{u}$, is calculated using linear, shallow water, wave theory relationships between surface elevation and horizontal velocities at the bed, and the Rayleigh wave height distribution

$$\overline{|\tilde{u}|} = \frac{1}{2}\left(\frac{g}{h}\right)^{1/2}\left[\int_0^\infty Hp(H)dH\right]\left[\frac{1}{T}\int_T|\cos(kx - \omega t)|dt\right] = \frac{1}{2}\left(\frac{g}{h}\right)^{1/2}\left[\frac{\sqrt{\pi}}{2}H_{rms}\right]\left(\frac{2}{\pi}\right). \quad (16)$$

Note that the constants multiplying H_{rms} in (16) are greater than the analogous constants for monochromatic waves (e.g., see Wu et al., 1985) by the factor $\pi/2$, because a distribution of waves is considered here.

Solving for the longshore current by substitution of $\tilde{S}_{yx}$ (12) and $\tau_y{}^b$ (15) into the longshore momentum relationship (13) and neglecting S'_{yx} yields

$$V = \frac{1}{\rho c_f\overline{|\tilde{u}|}}\frac{\sin\hat{\alpha}_0}{C_0}\langle\epsilon_b\rangle. \quad (17)$$

The terms $\langle\epsilon_b\rangle$ and $\overline{|\tilde{u}|}$ are given by (6) and (16), and (17) reduces to

$$V = \frac{3}{4}\frac{B^3 f_p g^{1/2}}{c_f\gamma^4}\frac{\sin\hat{\alpha}_0}{C_0}\frac{H_{rms}^6}{h^{9/2}}. \quad (18)$$

An analytical solution is obtained for a plane sloping beach limited to shallow water by simply substituting H_{rms} (9) into (18)

$$V = \frac{23}{20}\frac{g}{\pi^{1/2}}\frac{a^{1/5}}{c_f}\tan\beta\frac{\sin\hat{\alpha}_0}{C_0}h^{9/10}\times\left[1 - h^{23/4}\left(\frac{1}{h_0^{23/4}} - \frac{a}{r_0^{5/2}}\right)\right]^{-6/5}, \qquad 0 < h < h_0 \leq L/20 \quad (19)$$

with a and r_0 defined in (9). A maximum velocity occurs at about mid-surf zone, $V \to 0$ as $h \to 0$, and V is small for $h \sim h_0$. For general bottom profiles, V can be solved for by first numerically integrating for H_{rms} (8) and then substituting into (18).

The data (Table 1) show that $V/\overline{|\tilde{u}|} \sim O(1)$ at the location of maximum V within the surf zone. Therefore, the weak current assumption is not well met for this data. For the general case, but limiting the discussion to the condition of straight and parallel contours, the modulus of the total velocity in (14) is given by:

TABLE 1. Wave and beach conditions.

	February					
	2	3	4	5	6	Average
			At S_{yx} array			
h (m)	9.3	9.1	9.1	9.0	8.8	
f_p (Hz)	0.063	0.070	0.070	0.078	0.090	
[a] $\langle\hat{\alpha}(f_p)\rangle$ (°)	14.2	16.6	18.4	17.8	17.8	
[b] $\hat{\alpha}(f_p)$ (°)	14.0	17.9	19.7	19.2	15.1	
H_{rms} (m)	0.37	0.49	0.52	0.41	0.26	
$\tilde{S}_{yx}$ (J/m^2)	−38.9	−78.4	−88.9	−53.7	−21.4	
			At ~4 m			
h (m)	4.0	3.8	3.8	3.6	3.5	
[c] H_{rms} (m)	0.40	0.55	0.56	0.45	0.26	
[d] $\langle\hat{\alpha}(f_p)\rangle$ (°)	6.4	7.8	9.0	8.4	8.3	
			Surf zone			
Breaker Type	Plunge	Plunge	Plunge	Plunge/Spill	Plunge/Spill	
γ	0.46	0.48	0.45	0.43	0.34	0.43
$V_{max}/\lvert\vec{u}\rvert$	0.7	0.8	1.0	1.1	0.8	0.9
[e] Bottom slope	0.059	0.044	0.038	0.035	0.033	0.042
Foreshore slope	0.083	0.053	0.040	0.052	0.064	0.058

[a] Defined in Eq. (30).
[b] Defined in Eq. (29).
[c] Measured in ~4 m depth.
[d] Result of refracting the EMW to ~4 m depth; see text.
[e] Mean bottom slope measured between shoreline and mean breaker line.

$$|\vec{u}| = (V^2 + \tilde{u}^2 + 2V\tilde{u}\sin\hat{\alpha})^{1/2} \tag{20}$$

where the mean cross-shore velocity integrated over depth $U = 0$ by the continuity equation. The longshore velocity is composed of the mean longshore current plus the longshore wave component

$$v = V + \tilde{u}\sin\hat{\alpha}. \tag{21}$$

The general longshore bed shear stress formulation requires substituting (20) and (21) into (14) and averaging over the wave period for a particular wave height

$$\tau_y^b(H) = \frac{1}{T}\int_T \rho c_f(V^2 + \tilde{u}^2 + 2V\tilde{u}\sin\hat{\alpha})^{1/2} \times (V + \tilde{u}\sin\hat{\alpha})dt. \tag{22}$$

The ensemble average is then calculated

$$\tau_y^b = \int_0^\infty \tau_y^b(H)p(H)dH. \tag{23}$$

This results in a nonlinear equation which is difficult to solve since V and H cannot be brought outside the averaging integrals. The linear solution is used as the starting values for a numerical iterative solution, which was verified against the analytical solution for small angles of wave incidence. The numerical solution is described in appendix A.

For completeness, if the mean longshore current interaction with the wave field is significant, the mean velocity effects should be included in wave refraction:

$$V + \frac{C}{\sin\hat{\alpha}} = \frac{C_0}{\sin\hat{\alpha}_0}. \tag{24}$$

The refractive effects of the mean longshore current (24) were included in the model comparisons with data, but were found to change the results by less than one percent. Therefore, the results of including (24) will not be shown later.

The linearized analytical solution (19) and the more general solution including (23) result in smooth velocity distributions on planar beaches, which, as will be seen, can compare quite reasonably with observations. However, bathymetry which is not smooth (particularly barred profiles) can cause unreasonable undulations in the predicted velocity distributions. Therefore, the lateral transfer of turbulent momentum described by the integrated Reynold's stresses in (1) may sometimes be significant. Since the functional form of the integrated Reynold's stress is not known, it is usually parameterized using an eddy viscosity

$$S'_{yx} = \overline{\int_{-h}^{\eta} \rho u'v'dz} = -\rho\nu D\frac{dV}{dx} \tag{25}$$

where D is the total depth and ν is the kinematic eddy viscosity coefficient.

Bowen (1969) was the first to apply the eddy viscosity formulation (25) to the nearshore current problem and simply assumed ν constant. Subsequent authors have employed Prandtl's mixing length hypothesis

$$\nu = -|u'l'| \quad (26)$$

where u' and l' are characteristic velocity and length scales (e.g., Longuet-Higgins, 1970a, Thornton, 1970; Jonsson et al., 1974). Longuet-Higgins (1970a) suggested the mixing length should increase with distance from shore and the velocity intensity be characterized by the wave speed, such that

$$\nu = N|x|\sqrt{gh}, \quad \text{all } x \quad (27)$$

where N is an adjustable coefficient in the range $0 \leq N \leq 0.016$. Ostendorf and Madsen (1979) derived a similar form but based on the assumption that the characteristic velocity was the maximum velocity at the bed. Bowen and Inman (1974) compared various eddy viscosity formulations with values obtained from dye dispersion studies within the surf zone and from model fitting of the existing (limited) longshore current distributions. They concluded that the Longuet-Higgin's (1970a) formulation gives reasonable agreement with data. The present analysis will therefore use (25 and 27) in solving (13) when including eddy viscosity. Solutions with and without eddy viscosity will be considered below.

3. Field data

a. Experiment

The experiment was conducted at Leadbetter Beach from 30 January to 23 February 1980 as part of the Nearshore Sediment Transport Study (NSTS). The objective of NSTS was to use field experiments to formulate an improved littoral transport equation for topographically simple beaches. Verification and calibration of longshore current models are an integral part of the study. Field sites were selected where it could be reasonably assumed that near the shoreline the waves are homogeneous in the longshore direction and that bottom contours are relatively straight and parallel. These conditions greatly simplify the dynamical description and analysis. Two comprehensive, approximately one-month long experiments were conducted at Torrey Pines (north of San Diego) and Leadbetter (at Santa Barbara) Beaches, California. One difference between these and past experiments is that in the present experiments waves and currents were measured along a transect on a relatively simple, almost plane beach at relatively close spacings (compared with the wavelength of the dominant period). However, in our opinion the greatest difference between the present and past longshore current field experiments is not the density of surf zone current sensors, but rather the considerable emphasis placed on adequately measuring incident wave directional properties.

The beach at Leadbetter Beach is composed of well-sorted fine to medium size sand. The mean nearshore slope varied between 0.03 and 0.06 during the experiment, depending on the tide level and wave climate. Well-developed cusps occurred at the beginning of the experiment. No major offshore bar was apparent. The shoreline has the unusual east–west orientation along a predominantly north–south coast. The open-ocean waves are limited to a narrow window of approach (±9° centered on 249°) because of the protection from Point Conception to the north and the Channel Islands to the south. The generally highly directionally filtered ocean swell from the North Pacific approach the beach from almost due west, resulting in large oblique angles relative to the surf zone bottom contours.

We had trepidations about making measurements at Leadbetter Beach because of the generally very small waves and large Macrocystis kelp beds immediately offshore. The waves are usually small because the dominant open ocean waves are from the northwest, a direction from which Leadbetter Beach is well protected. The Macrocystis kelp can have stems in excess of 20 m and is one of the fastest growing plants on earth. During times of large waves, the kelp breaks loose and eventually ends up on the beach. It was anticipated that the kelp would become entangled in the instruments, greatly increasing their effective drag, resulting in broken or damaged instruments. Thus, it was expected that either there would only be small waves, in which case the experiment would be uninteresting, or that if there were large waves, instruments would be damaged because of the kelp problem.

As it turned out, the wave climate varied dramatically during the experiment. During the instrument installation, the waves were very low (which made the installation go very smoothly). The inshore instruments were installed on an essentially dry beach at spring low tides. The offshore instruments were installed by divers. The measurements were taken at high tide when all the instruments were submerged.

Measurements commenced on 30 January. During the first week the winds were generally light; consequently the incident waves were almost entirely derived from the deep ocean resulting in a narrow band swell. Rather long "sets" or wave groups were associated with the narrow-band waves, and plunging breakers were most often observed. In late afternoon of 6 February the barometric pressure started to drop, signaling the first of a three week series of storms which have been variously categorized as the 1-in-25 to 1-in-40 year storm event. Strong winds associated with these storms created a wind driven sea inside the Channel Islands from a range of directions; at the same time, a swell derived from the deep ocean was also present, often resulting in a bimodal or broad banded wave spectrum.

As many as 24 electromagnetic current meters and 14 pressure sensors were simultaneously deployed. The instruments were most densely spaced in the surf zone. The transect of instruments starting in 3 m depth is shown in Fig. 1. Instruments not shown in deeper water include a current meter at 5 m depth and an S_{yx} array (Higgins et al. 1981) composed of four pressure sensors

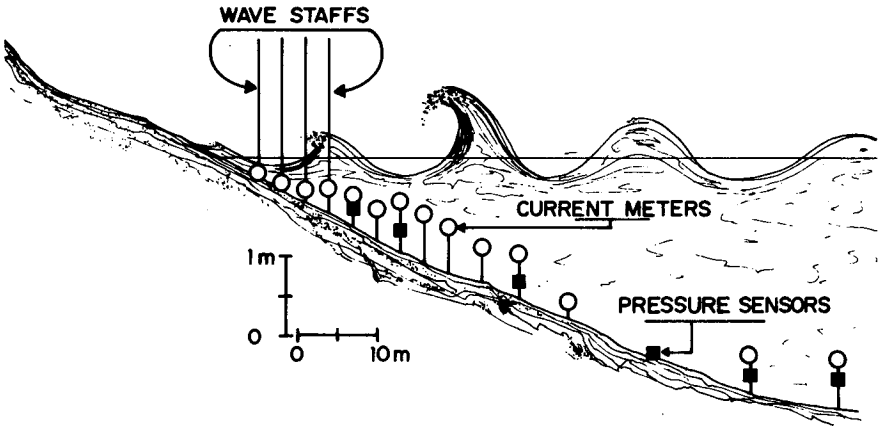

FIG. 1. Cross-shore array of current meters, pressure sensors and wave staffs.

at 9 m depth. A 14 sec wave is drawn to horizontal scale to show the waves were spatially well resolved. All instrument signals, either analog or PCM encoded, were cabled to shore where they were recorded.

The kelp problem was partially solved by positioning people updrift of the instruments to intercept the kelp. The kelp masses (referred to colloquially as "kelp monsters"), weighing up to several hundred pounds, were manually removed from the surf onto the beach. This procedure worked well for about two weeks, but eventually mother nature won out over our efforts.

Quality control over instrument orientation was maintained by checking all the surf zone current meters at the low tide prior to the high tide during which the measurements were taken. Since most of our measurements were made during daylight hours, many of the instrument checks were at night. Working at night in the surf zone, during times of large waves, can sometimes be rather intimidating!

We remark that the surf zone is an adverse environment in which to make measurements, and obtaining this dataset was a challenge. Out of the 24 electromagnetic current meters we started with, 17 were seriously damaged. Out of the eleven members of the dynamics team, six were injured, visiting either the emergency room or a doctor (fortunately nothing serious).

A basic assumption of the existing models is that the incident waves are narrow banded in frequency and direction. It was reluctantly conceded that only the narrow-band days occurring at the beginning of the experiment from 2 to 6 February are appropriate for the present model comparisons. The waves during this time were derived from a distant North Pacific storm so that the angle of wave incidence was restricted to the very narrow window from the west and swell spectra were narrow banded in frequency. Although the wave heights were relatively small (Table 1) the large incidence angles resulted in driving forces, $\tilde{S}_{yx}$, significant enough to generate moderately strong longshore currents ($\sim$0.5 m s^{-1}). Mean longshore currents during the storm events (not considered here) reached 1.5 m s^{-1}.

The bottom profiles for 2–6 February are shown in Fig. 2. Rod and level surveys of the beach profile were obtained at least daily by wading to approximately 50 m offshore. Complete bathymetric surveys (see Wu et

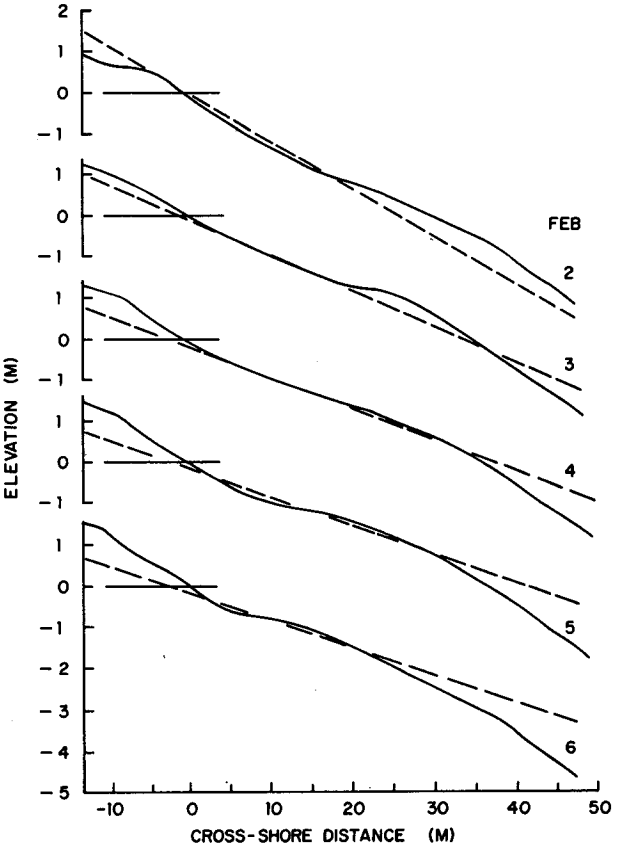

FIG. 2. Bottom profiles 2–6 February 1980; elevation and distance are zero at the mean shoreline location of each data run. The mean bottom slopes within the surf zone are indicated by dashed lines.

al., 1985; Fig. 2) composed of range lines at 50 m alongshore intervals extending from the beach to out past the 10 m depth contour, encompassing a region 600 m upcoast (west) and 1500 m downcoast (east), were conducted on 22 January and 25 February. The daily beach profiles and 22 January offshore profile are connected to give the complete profiles shown in Fig. 2. The 22 January offshore profile would not be expected to change very much up to at least 6 February, given the mild wave climate during this time.

A mean beach slope, $\tan\beta$, representing the plane sloping beach was determined by a least-square linear fit to the bottom profile across the surf zone. The surf zone profiles were nearly planar during 2–6 February. A foreshore slope was also determined and is always steeper than $\tan\beta$ (Table 1).

To apply a one-dimensional longshore current model, not only must the beach contours be essentially straight and parallel but the beach orientation must be accurately determined. A misalignment of the beach orientation can lead to substantial error in the radiation stress calculations (Guza and Thornton, 1978). The beach orientation was determined by fitting straight lines (in the least square sense) to the +50, 0 (MSL), −50 and −100 cm depth contours across measured profile lines and determining the average orientation for the four contours. An unresolved question is what is the approximate alongshore scale of longshore currents. However, the average alongshore orientation measured over 200 m (five profile lines at y = 100, 50, 10, −60, −100 m) and over 110 m (three profile lines at y = 50, 10, −60 m), were essentially the same. The beach orientation used in this analysis was averaged over 110 m for the 16 days from 29 January to 13 February. The average beach orientation varied little day to day during this time period (standard deviation = 0.43°). All angles given in Tables 1 and 2 are relative to the coordinate system determined in this manner.

Note that in a two-dimensional nearshore current analysis of this same data, Wu et al. (1984) used the original NSTS coordinate system, which is rotated 1.2° counterclockwise relative to the coordinate system used here. The results of a two-dimensional analysis are not dependent on the coordinate system employed.

b. *Incident wave parameters*

The longshore current models require specification of a characteristic incoming wave height, frequency, and direction. Directional information was obtained from the slope array, 610 cm on a leg, in 9 m depth (Higgins et al., 1981). Because the models assume a line spectrum in both frequency and direction, it is necessary to collapse the measured directional wave information into a single representative wave train. The $\tilde{S}_{yx}$ is universally hypothesized to be the primary forcing function for longshore currents, so a single angle and frequency are defined in such a way that $\tilde{S}_{yx}$ used in the model corresponds to the total measured value. Applying linear theory yields

$$\tilde{S}_{yx}(f) = \overline{\int_h^0 \rho\tilde{u}(f, z)\tilde{v}(f, z)dz}$$

$$= \int_\alpha E(f, \alpha)n(f)\sin\alpha\cos\alpha\, d\alpha \qquad (28)$$

where

$$n = \frac{1}{2}\left[1 + \frac{2kh}{\sinh 2kh}\right]$$

and α is the local angular deviation from normal incidence. Directional wave information at each frequency can be collapsed into a single representative direction by defining a "significant angle" at each frequency (Higgins et al., 1981)

$$\sin\hat{\alpha}(f)\cos\hat{\alpha}(f) = \tilde{S}_{yx}(f)/E(f)n(f). \qquad (29)$$

Using the frequency at the peak of the spectrum (f_p) as the representative frequency, the definition is extended to obtain a single representative direction for the entire spectrum

$$\langle\hat{\alpha}(f_p)\rangle = \frac{1}{2}\sin^{-1}[2\tilde{S}^T_{yx}/E^T n(f_p)] \qquad (30)$$

where E^T and $\tilde{S}^T_{yx}$ are the total energy density and radiation stress summed over the sea-swell band of frequencies (0.05–0.3 Hz). Equation (30) collapses the entire directional spectrum into a single plane wave at frequency f_p, which has the energy of the entire incident wave band and a direction $\langle\hat{\alpha}\rangle$ which yields the total measured $\tilde{S}^T_{yx}$. This simplification is only appropriate for spectra narrow banded in both frequency and direction.

The $\tilde{S}_{yx}$ is a conserved property for a nondissipative wave system propagating over straight and parallel contours. The contours inside about 5 m are straight and parallel to a good approximation, but the deeper contours are not. To confirm that the collapse of the full directional spectrum into a single wave train is not introducing large errors into the necessary refraction calculations, comparisons were made between refracting the "full" directional spectrum and the equivalent monochromatic wave [i.e., height = H_{rms}, frequency = f_p, direction = $\langle\hat{\alpha}(f_p)\rangle$; henceforth referred to as the "EMW"].

Full directional spectra for 5 and 6 February were calculated in 9 m depth using a modified maximum likelihood estimator technique with the constraint of accurately representing $\tilde{S}_{yx}(f)$ (S. Pawka, personal communication, 1984). Refraction to 3 m depth was performed using a version of Dobson's (1967) linear refraction program over the measured bathymetry. $\tilde{S}_{yx}(f)$ was calculated in 3 m using (28). The calculated $E(f)$ and $\tilde{S}_{yx}(f)$ spectra in 3 m depth for both days are narrow and the significant angle spectra, $\hat{\alpha}(f)$ (Eq. 29) are smooth (Figs. 3 and 4). The gradual increase in

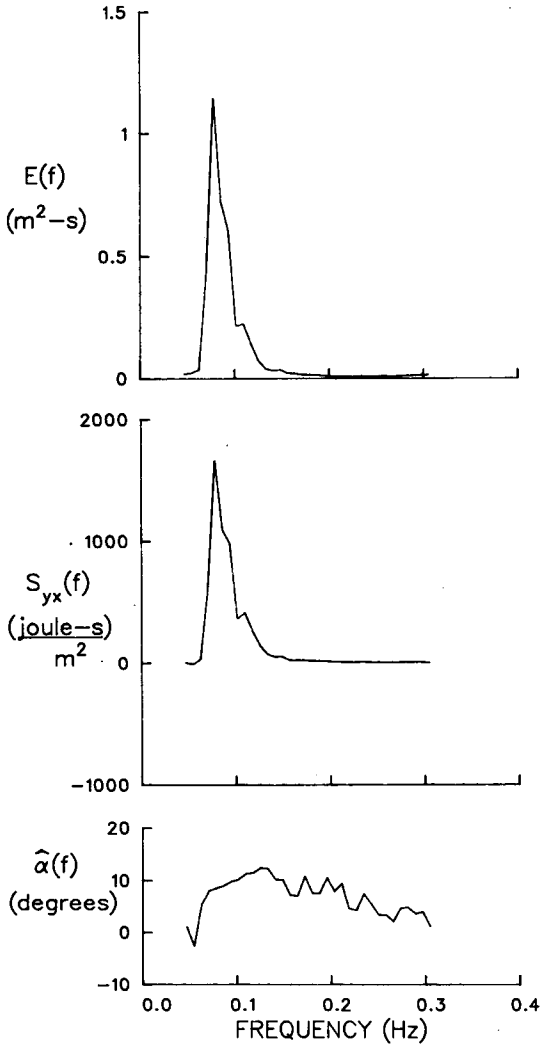

FIG. 3. Energy density, radiation stress density and $\alpha(f)$ spectra, 5 February 1980, $h = 3$ m.

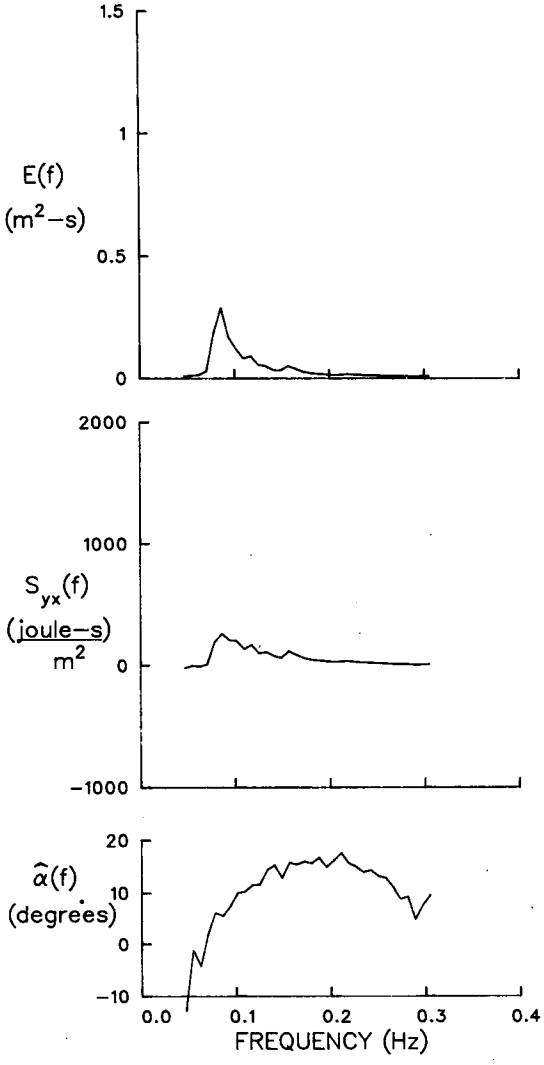

FIG. 4. As in Fig. 3 but for 6 February 1980.

significant angle with increasing frequency across the energetic region ($f \sim 0.1$ Hz) of the spectra is expected, for if all wave components were from the same direction in deep water, the lower frequencies would be more refracted toward normal incidence than the higher frequencies. Using these 3 m depth values of $E(f)$ and $\tilde{S}_{yx}(f)$ in (30) yields the "full" refraction estimates of $\langle\hat{\alpha}(f_p)\rangle$ given in Table 2. The 3 m depth values of $\langle\hat{\alpha}(f_p)\rangle$ obtained by refracting the single EMW from 9 m depth are also given. The similarity of EMW and full spectral refraction results suggests that only small refraction errors are introduced using the EMW, at least for these narrow banded wave days.

In principal, the refracted EMW could be used to provide all required wave input conditions [f_p, H_{rms}, $\langle\hat{\alpha}(f_p)\rangle$] for the longshore current models. However, a pressure sensor in 4 m depth is used to provide more accurate values of H_{rms}. A comparison of wave heights using EMW refraction and linear shoaling with measured values in 4 m showed the predicted waves were consistently larger by about 15 percent than the measured values. Thus, incident wave input conditions are specified in 4 m depth (always well outside wave breaking for this data) with $\langle\hat{\alpha}(f_p)\rangle$ obtained by EMW refraction and H_{rms} measured directly (Table 1). The

TABLE 2. Wave angles in 3 m depth. "Full" and "EMW" refer to angles based on spectral refraction and refraction of the equivalent monochromatic wave.

	Full	EMW
	$\langle\hat{\alpha}(f_p)\rangle$ (°)	$\langle\hat{\alpha}(f_p)\rangle$ (°)
Feb. 5	7.8	7.4
Feb. 6	7.5	7.4

depth contours inside 4 m depth are nearly plane parallel so further refraction is treated analytically.

Direct measurements of S_{yx} (gradients) in the surf zone would clearly be desirable, but the small wave angles make the gradient measurements highly sensitive to current meter orientation errors (Guza and Thornton, 1978). Even with proper sensor orientation, it is not clear that the directional response of the sensors is sufficiently well known to allow measurement of S_{yx} gradients.

The observed spatial variation of H_{rms} are shown in Fig. 5. Surface elevation was not measured directly, but was inferred using linear wave theory spectral transfer functions with either the pressure or current meter records as described in detail by Thornton and Guza (1982). After band-pass filtering between 0.05 and 0.5 Hz, wave heights were determined from 68 min surface elevation records using the "zero-upcrossing method." Since the average wave period was about 14 sec, the total number of waves in the 68 minute record was about 300. Empirical probability density functions and the height statistic of root-mean-square wave height, H_{rms}, were calculated from the ordered set of wave heights.

The wave height transformation models require specification of the breaker index, γ. The value of γ was determined from measured wave heights. Assuming $H_{rms} = \gamma h$ in the inner surf zone, the mean γ for all days is 0.43, which is nearly identical to the 0.42 obtained over a wide range of wave conditions at the Torrey Pines experiment (Thornton and Guza, 1982; Figs. 1 and 3). There is considerably more scatter (0.34–0.48) in the present data (Table 1). This may be partially due to the differences in breaker type at the two beaches. On the low slope ($\tan\beta \sim 0.02$) Torrey Pines Beach, the waves broke as spilling or mixed plunging/spilling. On the steeper Leadbetter Beach ($\tan\beta \sim 0.04$) the waves were sometimes clearly plunging (2–4 Feb) and sometimes of mixed type. Laboratory measurements suggest greater γ for plunging breakers (Battjes, 1974). Additionally, the Leadbetter Beach dataset includes swash measurements (where much of the scatter occurs), while the Torrey Pines data is from depths deeper than about 1 m. The linear wave theory transfer functions may not accurately transform velocities to surface elevations in the extremely shallow water of the swash. Finally, cusps at Leadbetter Beach definitely disturbed the nearshore flow. Any or all of these factors could cause the observed scatter.

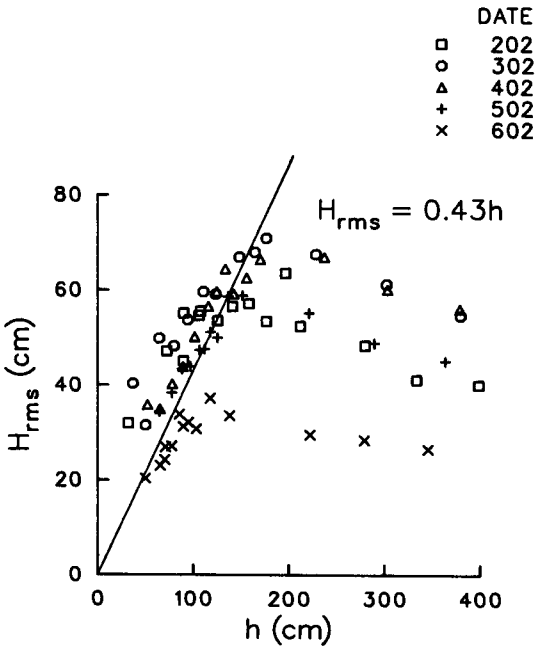

FIG. 5. H_{rms} wave height distribution compared with $H = 0.43h$ inside the surf zone.

The wave height transformations and longshore current formulations are next compared with the field data.

4. Model comparisons with measurements

Wave height transformation over measured bathymetry are compared with observations in Fig. 6. The input wave parameters of H_{rms}, mean wave direction $\langle\hat{\alpha}(f_p)\rangle$ and frequency at the peak spectral peak, f_p, are specified at depth $h \sim 4$ m (Table 1). The daily measured γ values (Table 1) are used in the models. Optimal B values calculated using a least-square error criteria between theory and data, and the average percent difference between observations and predictions are given in Table 3. The average least-square error for H_{rms} predictions ranged between 5–13% with an average of 9% for the 5 days, values similar to the Torrey Pines Beach data (Thornton and Guza, 1983).

The longshore current models for linearized $\tau_y{}^b$ are presented first. Here and in all subsequent results, optimal c_f (and N) coefficients are determined by iteratively solving for the least square error between calculated and measured longshore current values shoreward of the mean breaker line. The analytical models for longshore current and H_{rms} distributions assuming a planar beach and no eddy viscosity ($N = 0$), are compared with 4 February data in Fig. 7. The analytical solutions for wave height and longshore current distributions can give quite reasonable comparisons with field measurements provided the beach is approximately planar (See Fig. 2) and the appropriate γ, B and c_f values are used.

Longshore current distributions over actual bathymetry for linearized $\tau_y{}^b$, with and without eddy viscosity, are compared with observations in Fig. 8. The inclusion of eddy viscosity does not significantly improve the comparisons with data. Again, optimal coefficients are determined by iteratively solving for the least-square error between calculated and measured

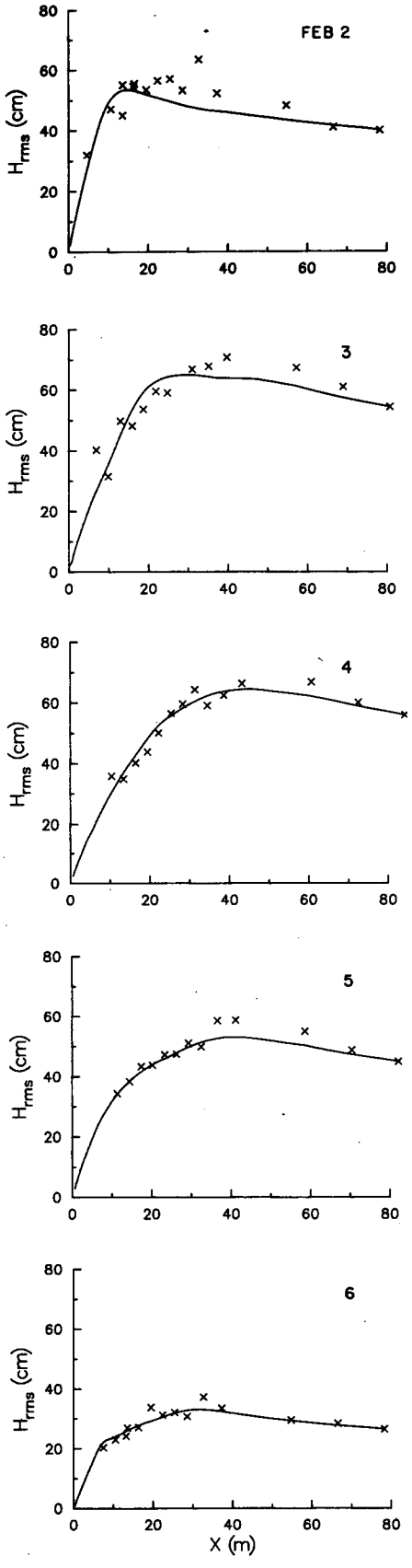

TABLE 3. Wave transformation model parameters and percent errors.

	February					
	2	3	4	5	6	Average
[1] U_r	13	14	14	9	4	11
[2] ξ_0	1.85	1.06	0.91	0.84	0.90	
B	0.8	0.9	1.1	1.1	1.0	1.0
% error	12	13	7	5	6	8.6

[1] $U_r = ak/(kh)^3$; at $h \sim 4$ m.
[2] $\xi_0 = \tan\beta(H_{rms}/L_0)^{1/2}$; H_{rms} @ $h \sim 4$ m, deep water wave length L_0.

longshore current values shoreward of the mean breaker line. The generally small currents observed seaward of the mean breaker line were not included in the least-square error analysis because of the relative large errors from sensor calibration and tidal and shelf current contamination. In any event, the inclusion of these observations changes the results very little. Note that the present procedure of a least squares fit of data does not work well on 2 February for which a large error is calculated because of the lack of observations at the nearshore. Only a few points are used in the curve fitting, and additional measurement locations close to shore probably would have resulted in much different coefficients and calculated error. Therefore, the results of 2 February are not included in the average values (Table 4).

Although quite reasonable comparisons can be obtained using a linearized τ_y^b, the strength of the longshore current relative to the magnitude of the wave induced bottom velocity, are O(1) (Table 1), suggesting that linearization of the bottom friction is not appropriate. Longshore current solutions for linear and nonlinear τ_y^b with $N = 0$ are compared in Fig. 9. The nonlinear, and presumably more physically correct τ_y^b increases the bottom stress compared with the linear τ_y^b, i.e., for the same c_f value, the nonlinear τ_y^b decreased the predicted longshore currents. The effect of the nonlinear τ_y^b increases with increasing V. The resulting best fit c_f values for nonlinear τ_y^b are decreased on the average by one-third compared with the corresponding linear τ_y^b (Table 4). Using the best fit c_f values results in similar velocity distributions, but with the nonlinear τ_y^b, the velocity distribution is broadened with slightly increased velocities both shoreward and seaward of the mean breakerline (Fig. 9). The nonlinear τ_y^b formulation gives a slightly improved fit.

5. Discussion and conclusions

Models of longshore currents generated by obliquely incident narrow-band random waves are calibrated

FIG. 6. Wave height transformation (solid line) on real bathymetry compared with measurements.

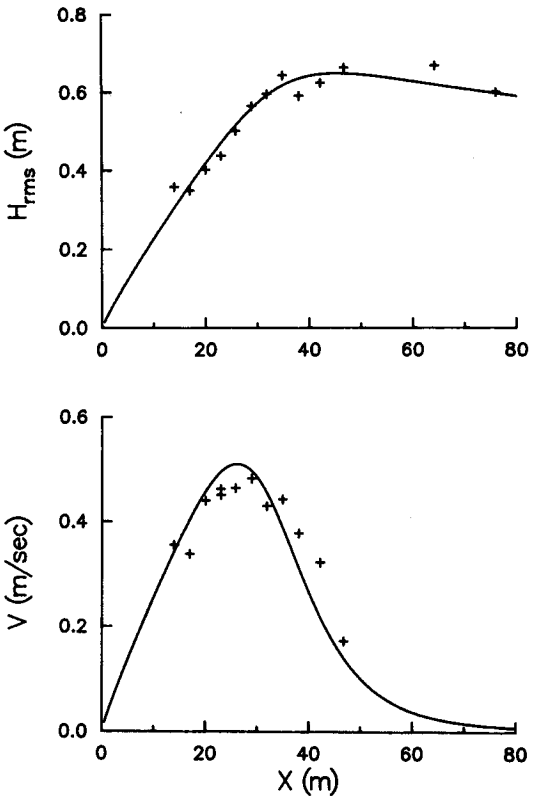

FIG. 7. Analytic solution for H_{rms} and V on planar beach compared with measurements, 4 February 1980.

against extensive field data acquired at Santa Barbara, California. The wave angles at breaking were moderately large ($\alpha_b \sim 5°$) resulting in sometimes strong longshore currents (up to 0.5 m s^{-1}) depending on the wave height. The waves for the selected five days were very narrow banded in both frequency and direction in keeping with the model assumption. Measurements consisted of a cross-shore transect of current meters and wave sensors at close intervals compared with the dominant wave length. The radiation stress and wave directional spectra were measured in 9 m depth. The waves were numerically refracted to the 4 m contour inside of which the bottom contours could be reasonably assumed straight and parallel, and at times almost planar, further simplifying the analysis.

Shorewards of the 4 m depth, the random wave transformation model is used as input to the longshore current models. The transformation model ingredients are linear wave shoaling and wave dissipation described by "classical" periodic bore theory. Important deficiencies include the approximate nature of the bore dissipation model and the somewhat arbitrary form of the breaking wave distribution weighting function [$W(H)$, Eq. (5)]. These shortcomings in the shoaling theory are partially compensated for by adjusting the B coefficient in the bore dissipation function. The

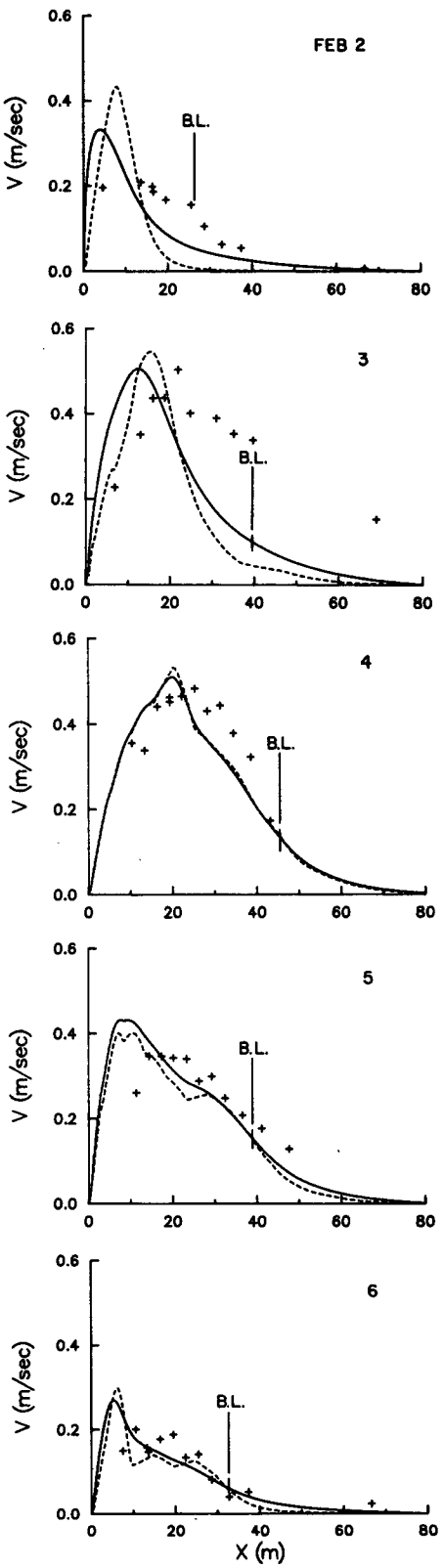

FIG. 8. Comparison of Longshore current distributions for linear τ_y^b on actual bathymetry with (solid line) and without (dashed line) eddy viscosity.

TABLE 4. Longshore current model coefficients, c_f and N, and percent errors.

	February					
	2	3	4	5	6	Average
			Linear τ_y^b analysis			
Plane bottom, $N = 0$						
c_f	0.010	0.009	0.009	0.009	0.010	0.009*
% error	67	48	15	19	18	25*
Actual bottom, $N = 0$						
c_f	0.010	0.009	0.009	0.008	0.009	0.009*
% error	74	54	18	24	33	32*
Actual bottom, $N \neq 0$						
c_f	0.005	0.007	0.009	0.007	0.008	0.008*
N	0.017	0.004	0.0001	0.0004	0.002	0.002*
% error	50	51	18	24	28	30*
			Nonlinear τ_y^b analysis			
Actual bottom, $N = 0$						
c_f	0.0075	0.0060	0.0055	0.0055	0.0070	0.006*
% error	71	49	15	17	36	29*

* February 2nd values not included in average values.

model is reasonably robust, as Thornton and Guza (1983) showed that a 25 percent variation in B resulted in less than a 10 percent increase in the rms error of the predicted wave heights. The value of B is a measure of breaker intensity and it is expected that $B \leq 1$. The optimal values of B ranged between 0.8 and 1.1 (Table 3). Optimal B values were about 1.5 at Torrey Pines Beach (Thornton and Guza, 1983). The fact that B has approximately the correct magnitude indicates that the cumulative error of the other assumptions is not extremely large; B values greater than 1.0 are also consistent with laboratory results with monochromatic waves showing that linear bore theory underestimated dissipation by 30–50% (Stive, 1983).

The least-square error calculations were unweighted with respect to the spatial distribution of measurement locations. Since the measurements were more densely spaced inshore, the resulting B values and wave height distributions are biased to give a better fit with the data in the inshore region. With optimal B values, the theory underpredicts H_{rms} offshore and overpredicts H_{rms} inside the surf zone (Fig. 6).

In the model, B is assumed constant. In fact, the intensity of breaking varies spatially because of a dependence on the local beach slope, wave steepness and relative depth. Casual observations indicate that the infrequent breaking waves offshore in relatively deep water are usually spilling, while more intense plunging breakers are typical in shallower water, particularly over a bar; waves in the inner surf zone are usually spilling. Thus, both the distribution (percent) of breaking waves and their intensity vary spatially. Not enough is known about B to include meaningful spatial variation in the model.

It is apparent from (8) that B values are dependent on the γ values chosen since the ratio (B^3/γ^4) occurs as an isolated term. Increasing γ results in an increasing B value. A single combined empirical coefficient could have been defined, but it is hoped that by retaining γ and B separately, the components of the model might be better understood. An attempt was made to relate the B and γ coefficients to the Ursall number and the Iribarren Number, $\xi_0 = \tan\beta(H_0/L_0)^{-1/2}$, (Table 3) as was suggested by Stive (1983), and also to $\tan\beta$ and H_0/L_0 separately. The only apparent correlation is the increase in γ with increasing $\tan\beta$, which is similar to the observations by Sallenger and Holman (1985).

The longshore current models incorporate various simplifying assumptions. Good comparisons with data were obtained for all models by adjusting the free parameters of c_f and N used in the bottom shear stress and eddy viscosity formulations. An objective here is to determine appropriate c_f and N values. In previous longshore current models, Thornton (1970) used a value for c_f that depended on wave velocity and bed roughness (Johnson, 1966); Longuet-Higgins (1970b) simply used $c_f = 0.01$ based on limited wave and hydraulic channel studies. Shemdin et al. (1978) compiled values of c_f for various field studies of wave dissipation, and reported values ranging between 0.005 to 0.3. Thornton and Guza (1981) obtained $c_f = 0.01 \pm 0.01$ averaged over four days by equating measured S_{yx} gradients with longshore bed shear stress (Eq. 1); the large uncertainty in the measured c_f value is due to the statistical noisiness of directly measured S_{yx} values. Newer theoretical formulations have been suggested (e.g., Grant and Madsen, 1982). In the present work, c_f is taken as a constant (i.e., not a function of local wave or bed roughness parameters).

The inclusion of the nonlinear $\tau_y{}^b$ in the formulation is significant, with increasing importance as wave height and V increase. A least square fit of the longshore current solution inside the mean breakline resulted in an optimal bed shear stress coefficient, $c_f = 0.009 \pm 0.001$,

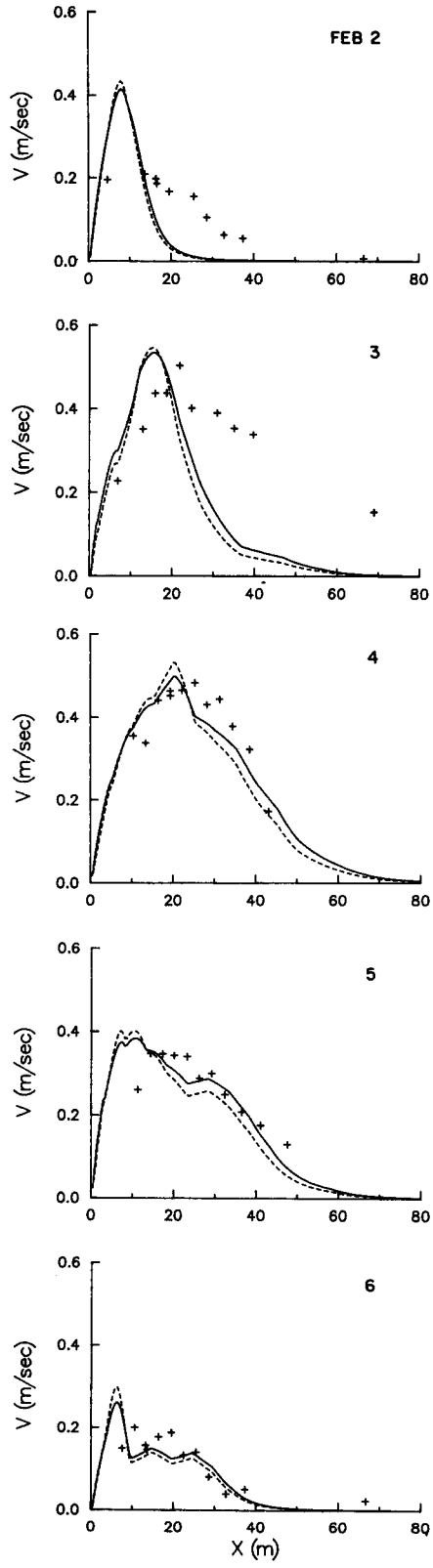

FIG. 9. Comparison of longshore current distributions for linear (dashed line) and nonlinear (solid line) τ_y^b. Eddy viscosity is not included ($N = 0$), and measured bathymetry is used.

for linear τ_y^b, comparable to previously suggested values. With fixed c_f, the nonlinear τ_y^b, decreased V_{max} (compared with using linear τ_y^b) from 11 to a maximum of 22 percent. The best fit c_f values for nonlinear τ_y^b are 0.006 ± 0.0007, significantly less than for linear τ_y^b. The shape of the longshore current distributions are virtually the same for linear and nonlinear τ_y^b when using optimal c_f for each case.

Good comparison of the predicted and measured velocities were obtained without including eddy viscosity. The gradual change in energy dissipation gives a gradual change in S_{yx}, and results in a smooth longshore current distribution. For completeness, eddy viscosity (after Longuet-Higgins, 1970a) was included; the optimal N values were small with an average of 0.002 and their inclusion did not significantly improve the linear model fits. The fact that a random wave model does not require eddy viscosity to predict currents on the present nearly planar bathymetry does not imply that turbulent horizontal Reynold's stresses are always unimportant in surf zones. Our point is that values of eddy viscosity obtained in nonrandom models do not necessarily correspond to actual Reynold's stresses, but may instead be parameterization of randomness.

For small angle of wave incidence and weak currents, the plane beach analytic solutions are comparable to the numerical solutions on real topography with or without eddy viscosity. Thus, the analytic solutions may be useful for many situations. Because of its greater internal consistency, and fewer free parameters (c_f only), the random wave driven model with nonlinear τ_y^b and $N = 0$ is our choice for general applications.

Acknowledgments. This analysis was supported by the Office of Naval Research, Coastal Sciences Branch, under Contract NR 388-114 (E. B. Thornton), and by NSF Grant OCE-8213657 (R. T. Guza). The Sea Grant Nearshore Sediment Transport Study (number R/CA-N-4D) and ONR supported the data collection. R. J. Seymour obtained the bathymetric data. The staff of the Shore Process Laboratory (Scripps Institution of Oceanography) installed and maintained the offshore sensors and data acquisition system. R. L. Lowe was the principal engineer. D. M. Burych performed the numerical analysis. R. A. Dalrymple, J. Kirby, K. O. McCoy, and others contributed substantially to the sensor maintenance at Santa Barbara. Their generous and untiring efforts are greatly appreciated. S. Pawka calculated the directional spectra and refraction transformations. Sadly, Steve died of cancer on 7 October 1983 after a hard fight. Oceanography lost a good scientist. The world lost a gentleman.

APPENDIX A

Numerical Calculation of Nonlinear τ_y^b

The longshore current with nonlinear τ_y^b is solved independently at each location based on a calculated

H_{rms} value. For a given location, (8) is solved for H_{rms} using the first order Euler method. The difficulty of solving for V using nonlinear $\tau_y{}^b$ is that V cannot be explicitly brought outside the double integral of $\tau_y{}^b$ [Eqs. (22) and (23)], which is averaged over time and integrated over all H. Since V is not a function of time, it can be brought outside the time averaging integral of (22)

$$\tau_y{}^b(H) = \frac{V}{T}\int_T \rho c_f(V^2 + \tilde{u}^2 + 2V\tilde{u}\sin\hat{\alpha}) \times \left(1 + \frac{\tilde{u}}{V}\sin\hat{\alpha}\right) dt = Vf(V, H). \quad \text{(A1)}$$

Neglecting the turbulent momentum flux S'_{xy}, the following iterative solution of (13) is used

$$V^{i+1} = \frac{-\sin\hat{\alpha}_0}{C_0}\langle\epsilon_b\rangle \Big/ \int_0^\infty f(V^i, H)p(H)\,dh \quad \text{(A2)}$$

where i indicates the iteration and $\langle\epsilon_b\rangle$ is specified by (6). The initial V^1 is obtained from the linear solution (18). The iteration was carried out until the absolute value of the change in V was less than $\epsilon = 0.01$. An absolute error (as opposed to a relative error) across the surf zone was considered adequate and reduced the number of iterations required for values of V close to zero.

Within each iteration, the improper integral in (A2) must be evaluated. This was accomplished using Simpson's Rule starting at $H = 0$ and progressing in steps of ΔH. At each step, the closed integral of $\tau_y{}^b(H)$ in Eq. (A1) was evaluated using Simpson's Rule with 16 steps (only eight evaluations were required due to the symmetry of the integrand). A reasonable cutoff criterion for the improper integral had to be determined. The criterion to stop when the change in the partial summation is small does not work well since the change is a function of the stepsize ΔH. It was found that the integrand is quickly dominated by the scaled $1/H^2$ function

$$q(H) = \frac{H_{rms}/30}{H^2}. \quad \text{(A3)}$$

Once the integrand function goes below this curve, an upper limit can be put on the residual of the integral by integrating $q(H)$ from the value of H to ∞. By requiring that the integrand function be less than $q(H)$ and H be greater than $H_{rms}/0.3$, the residual of the integral will always be less than 0.01.

REFERENCES

Battjes, J. A., 1972: Set-up due to irregular waves. *Proc. 13th Int. Coastal Engineering Conf.*, New York, Amer. Soc. Civil Eng., 1993–2004.

——, 1974: Surf similarity. *Proc. 14th Int. Coastal Engineering Conf.*, New York, Amer. Soc. Civil Eng., 466–480.

——, and J. P. F. M. Janssen, 1978: Energy loss and set-up due to breaking of random waves. *Proc. 16th Int. Coastal Engineering Conf.*, New York, Amer. Soc. Civil Eng., 569–578.

Bowen, A. J., 1969: The generation of longshore currents on a plane beach. *J. Mar. Res.*, **27**, 206–215.

——, and Inman, D. L., 1974: Inshore mixing due to waves and wave-induced currents. *Symp. on Physical Processes Responsible for the Dispersion of Pollutants in the Sea with Special Reference to the Nearshore Zone. Rapp. P.-V. Reun.-Cons. Int. Explor. Mer*, 6–12.

Collins, J. I., 1970: Probabilities of breaking wave characteristics. *Proc. 13th Int. Coastal Engineering Conf.*, New York, Amer. Soc. Civil Eng., 399–412.

Dobson, R. S., 1967: Some applications of a digital computer to hydraulic engineering problems. Tech. Rep. 80, Stanford University, 172 pp.

Grant, W. D., and O. S. Madsen, 1982: Movable bed roughness in unsteady oscillatory flow. *J. Geophys. Res.*, **87**, 469–481.

Guza, R. T., and E. B. Thornton, 1978: Variability of Longshore Currents. *Proc. 16th Int. Coastal Engineering Conf.*, New York, Amer. Soc. Civil Eng., 756–775.

Hwang, L. S., and D. Divoky, 1970: Breaking wave set-up and decay on gentle slopes. *Proc. 12th Int. Coastal Engineering Conf.*, New York, Amer. Soc. Civil Eng., 377–389.

Higgins, A. L., R. J. Seymour and S. S. Pawka, 1981: A compact representation of ocean wave directionality. *Appl. Ocean Res.*, **3**, 105–111.

Jonsson, I. G., 1966: Wave Boundary Layers and Friction Factors. *Proc. 10th Int. Coastal Engineering Conf.*, New York, Amer. Soc. Civil Eng., **1**, 127–148.

Jonsson, I. G., O. Skorgaard and P. S. Jacobsen, 1974: Computation of longshore currents. *Proc. 14th Conf. on Coastal Engineering*, ASCE, 699–714.

Longuet-Higgins, M. S., 1970a: Longshore currents generated by obliquely incident sea waves, 1. *J. Geophys. Res.*, **75**, 6778–6789.

——, 1970b: Longshore currents generated by obliquely incident sea waves, 2. *J. Geophys. Res.*, **75**, 6790–6801.

——, and R. W. Stewart, 1964: Radiation stresses in water waves: A physical discussion, with applications. *Deep Sea Res. II*, 529–562.

Ostendorf, D. W., and O. S. Madsen, 1979: An analysis of longshore current and associated sediment transport in the surf zone. Rep. 241, Parsons Laboratory, Dept. Civil Engineering, Massachusetts Institute of Technology.

Sallenger, A., and R. Holman, 1985: Wave-energy saturation on a natural beach of variable slope. *J. Geophys. Res.*, **90**, 11 939–11 944.

Shemdin, O. H., K. Hasselman, S. V. Hsiao and K. Herterich, 1978: Nonlinear and linear bottom interaction effects in shallow water. *Turbulence Fluxes Through the Sea Surface, Wave Dynamics and Prediction*, A. Favre and K. Hasselmann, Eds., Plenum, 347–372.

Stive, M., 1983: Energy dissipation in waves breaking on gentle slopes. *J. Coastal Eng.*, **8**, 99–127.

Thornton, E. B., 1970: Variation of longshore current across the surf zone. *Proc. 12th Int. Coastal Engineering Conf.*, New York, Amer. Soc. Civil Eng., 291–308.

——, 1979: Energetics of breaking waves within the surf zone. *J. Geophys. Res.*, **84**, 4931–4938.

——, and R. T. Guza, 1981: Longshore currents and bed shear stress. *Proc. Conf. on Directional Wave Spectra Applications*, New York, Amer. Soc. Civil Eng., 147–164.

——, and ——, 1982: Energy saturation and phase speeds measured on a natural beach. *J. Geophys. Res.*, **87**, 9499–9508.

——, and ——, 1983: Transformation of wave height distribution. *J. Geophys. Res.*, **88**, 5925–5938.

Wu, C. S., E. B. Thornton and R. T. Guza, 1985: Waves and longshore currents: Comparison of a numerical model with field data. *J. Geophys. Res.*, **90**, 4951–4958.